International Journal of Pharmacology

ISSN 1811-7775

science alert

ansinet
Asian Network for Scientific Information

OPEN ACCESS International Journal of Pharmacology

ISSN 1811-7775
DOI: 10.3923/ijp.2025.295.316

Research Article
Exploring the Therapeutic Mechanism of Artesunate Against Ulcerative Colitis via Network Pharmacology and Molecular Docking

[1]Dike Zhao, [2]Shuting Wen, [1]Jun Niu, [3]Qiang Wang, [4]Hong Mi and [4]Fengbin Liu

[1]School of Traditional Chinese Medicine, Henan University of Chinese Medicine, Zhengzhou, 450046, China
[2]The First Clinical College, Guangzhou University of Chinese Medicine, Guangzhou, 510000, China
[3]Department of Traditional Chinese Medicine, Yangjiang People's Hospital, Yangjiang, 529500, China
[4]Department of Gastroenterology, The First Affiliated Hospital of Guangzhou University of Chinese Medicine, Guangzhou, 510000, China

Abstract

Background and Objective: Refractory ulcerative colitis has few effective drugs and an unknown etiology. Artesunate, an artemisinin derivative, may decrease colon inflammation in animal models via immunomodulation, although its targets and mechanisms are unclear. This study predicted artesunate targets, processes and effectiveness in treating ulcerative colitis using network pharmacology, molecular docking and animal trials. **Materials and Methods:** Artesunate and ulcerative colitis gene targets were searched in databases. The KEGG pathway enrichment and gene ontology analysis evaluated possible targets. Artesunate was evaluated in C57 mice with 3% dextran sodium sulphate-induced ulcerative colitis. Target gene expression was shown by western blotting, Haematoxylin and Eosin (H&E) staining, RT-PCR and immunohistochemistry. **Results:** Overall, network pharmacology evaluated 154 artesunate drug targets and 2,104 ulcerative colitis targets. The intersection of these objectives has 29 candidates. These targets controlled apoptosis, p53 and JAK/STAT signalling. The final validation targets were IL-6 and TP53 using molecular docking studies. In mouse models, artesunate reduced dextran sodium sulphate-induced weight loss, colon length, disease activity index and pathological scores and increased TP53 and decreased interleukin-6 expression in ulcerative colitis colon tissues. In the colon, artesunate activated Bax and Caspase-3 and downregulated STAT3 and Bcl-2. **Conclusion:** Network pharmacology and molecular docking identified artesunate's ulcerative colitis targets and processes. Artesunate decreased colon edema and damage in 3% dextran sodium sulphate-treated rats. To induce these effects, TP53 and interleukin-6 may control apoptosis and inflammation. Current findings might lead to ulcerative colitis medications.

Key words: Artesunate, ulcerative colitis, IL-6, TP53, immunomodulation, network pharmacology, molecular docking

Citation: Zhao, D., S. Wen, J. Niu, Q. Wang, H. Mi and F. Liu, 2025. Exploring the therapeutic mechanism of artesunate against ulcerative colitis via network pharmacology and molecular docking. Int. J. Pharmacol., 21: 295-316.

Corresponding Author: Fengbin Liu, Department of Gastroenterology, The First Affiliated Hospital of Guangzhou University of Chinese Medicine, Guangzhou, 510000, China

Competing Interest: The authors have declared that no competing interest exists.

Data Availability: All relevant data are within the paper and its supporting information files.

INTRODUCTION

Ulcerative colitis (UC) is a common refractory disease of unknown aetiology with a high frequency of relapse. At present, specific therapeutic drugs for UC are lacking. Drugs commonly used for the treatment of UC, such as aminosalicylic acid, glucocorticoids and immunosuppressants, have various limitations, such as high toxicity and recurrence after drug withdrawal. Traditional Chinese medicines and extracts have been used for the treatment of UC with significant curative effects, low recurrence rate, toxicity and few side effects, providing a promising alternative to conventional drugs.

Artesunate (ART), a derivative of artemisinin, is derived from the traditional Chinese medicinal herb *Artemisia annua* L. (Asteraceae). As the preferred antimalarial drug recommended by the World Health Organization, ART shows a high efficacy, rapid effect, multiple routes of administration and low toxicity. Since its discovery, ART has been used to treat *Plasmodium falciparum* malaria and rescue cerebral malaria[1]. In addition to the antimalarial effect with high efficiency and low toxicity, ART can promote tumour cell apoptosis[2], protect against inflammation[3] and contribute to immune regulation[4], among other functions, demonstrating broad pharmacological effects. The ART can alleviate colonic inflammation in animal models via immunomodulatory effects[5]; however, its targets and mechanisms remain undetermined.

Continuous advances in systems biology and bioinformatics have led to increased interest in the application of network pharmacology and molecular docking technologies to the development of new uses of marketed drugs and research on traditional Chinese medicine[6]. In this study, network pharmacology was used to predict the potential targets of ART in the treatment of UC and molecular docking technology was used to further screen for the potential targets involved in the drug-target-disease network based on binding ability. Finally, animal experiments were performed to verify the efficacy of ART in the treatment of UC, validate the accuracy of the screened targets and determine the molecular mechanisms. By clarifying the molecular mechanisms underlying the effects of ART, these findings provide a clear basis for expanding its application in clinical settings.

MATERIALS AND METHODS

Study area: The experiment was conducted in the First Affiliated Hospital of Guangzhou University of Chinese Medicine, China, between June, 2023 and September, 2023.

Prediction of ART targets: The ChEMBL database[7], Swiss Target Prediction database[8], Target-Prediction database[9] and PharmMapper online server[10] were combined in a four-in-one approach to search for potential targets of the ART drug monomer. The targets predicted by these methods were then sorted and imported into the UniProt database[11]; the official name of each gene was corrected after limiting the species to *Homo sapiens*. Duplicate targets obtained by the three prediction methods were removed and the remaining targets were recorded as potential targets of the ART drug monomer.

Searching for UC targets: The TTD[12], PHARMGKB[13], OMIM[14], GAD[15], DiGSeE[16], PALM-IST[17], PolySearch2[18], COREMINE[19] and a GEO chip analysis was used to preliminarily search for UC targets. The identified UC targets were consolidated, duplicate targets obtained by the three methods were removed and the disease-related targets for UC were obtained. After the names of the targets were corrected, target information was recorded for further analysis.

Construction of a PPI network: The STRING database[20] was used to construct protein-protein interaction (PPI) networks of the ART and UC targets. The intersection of the key targets of ART and UC was further obtained by the Venny 2.1 online platform and used to construct a PPI network to screen for potential targets of ART in the treatment of UC. Then, Cytoscape[21] was used for a visual analysis.

Gene ontology and KEGG pathway enrichment analyses: The GenCLiP database[22] was used to complete a gene ontology (GO) analysis and Kyoto Encyclopaedia of Genes and Genomes (KEGG) pathway enrichment analysis of the target genes. The gene names (official gene symbols) of the potential targets of ART for the treatment of UC were entered into the GenCLiP database for search retrieval and the GO Analysis and Pathway Analysis options were used.

Molecular docking analysis of potential targets: The molecular structure of the ART monomer was obtained from the DrugBank database[23]. The molecular structure of the protein-ligand complex structure of the target protein was obtained from the PDB database[24]. The POCASA1.1[25] was used to predict the active site of the target protein. The PyMOL was further used to remove redundant protein chains, original ligands, water molecules and small molecules in the obtained target protein receptor-ligand complex and a pdb format file of the target receptor protein was generated. The receptor file was imported into AutoDockTools[26], neutral hydrogenation was completed, the charge was calculated and the ligand atomic force field was defined as AD4 type. The PDBQT format

file for each target protein receptor was generated and docked with the ART monomer molecule in the pdbqt format. During docking, the grid interval was uniformly set to 0.375 Å. The built-in Lamarckian genetic algorithm (LGA) of AutoDock 4.2.6 was used. The number of runs for each docking setting was set to 10, the maximum number of evaluations was set to 2,500,000 and default settings were used for other parameters. After the docking was completed, the binding energies (BE) were sorted and the conformation with the smallest BE in each class was used to generate the ligand-protein complex in pdb files. A visual analysis was performed using PyMOL and LigPlot[27].

Experimental animals: A total of 48 SPF male C57 mice (6-8 weeks old, 30±3 g) were purchased from Guangdong Medical Laboratory Animal Center (Foshan, Guangdong) and raised in the SPF animal laboratory of the Laboratory Animal Center of the First Affiliated Hospital of Guangzhou University of Chinese Medicine. The mice were grouped using a random number table. A numbered table is composed of ten numbers from 0 to 90 randomly generated by the computer and each number has the same probability of appearing in the table. Grouping is, you need to use this tool to achieve random allocation. The experimental mice were housed in a rearing room at 22-24°C, relative humidity of 45±5% and 12 hrs alternating light/dark conditions. Experiments were started after 1 week of adaptive feeding with SPF mouse feed provided by the Guangdong Medical Laboratory Animal Center.

Ethical consideration: All animal experiments were approved by the Animal Ethics Committee of the First Affiliated Hospital of Guangzhou University of Chinese Medicine (20231125678).

Model preparation and drug administration: The mice were randomly divided into four groups (n = 12 per group): Control group (normal control group), dextran sodium sulphate (DSS) group (model group), SASP group (sulfasalazine drug administration group) and ART group (artesunate drug administration group). Following a previously described method of Nunes *et al.*[28], the mouse model of acute UC was established using 3% DSS (MW 36000-50000; MP Biomedicals, Irvine, California, USA, batch number: Q3526). A new 3% DSS aqueous solution was reconstituted daily and placed in a mouse drinking bottle for free access for 7 days to induce UC, except in the control group.

In each experimental group, 3% DSS was administered by gavage 8 hrs after the initial supply of 3% DSS modelling solution. The SASP group was treated with 200 mg/kg/day by gavage. The ART group was administered 75 mg/kg/day ART (Shanghai Yuanye Bio-Technology Co., Ltd., batch number: S16D8W50820) by gavage. The Control and DSS groups received normal saline by gavage. After continuous modelling and administration for 7 days in each group, samples were collected on the 8th day. The mice were sacrificed by cervical dislocation after fasting for 6 hrs. The complete cecum to rectum was placed on ice and the adhering adipose tissue on the intestinal segment was removed. Images were obtained and the lengths of the colon were recorded. The residual faeces in the intestinal tube were further washed with normal saline and the 1 cm intestinal segment at the junction of the colorectum was taken and immersed in 10% formalin solution for pathological examination. The remaining intestinal segments were transported in liquid nitrogen and stored in a -80°C refrigerator for subsequent testing.

Determination of the disease activity index score: The percentage of body weight loss, stool viscosity and faecal occult blood were evaluated daily during the dosing experiment as per the following previously described methods[29-31]. The disease activity index (DAI) was calculated using the formula:

$$DAI = \frac{\text{Weight loss score+Stool viscosity score+Faecal occult blood score}}{3}$$

Histological analysis and immunohistochemistry: The colon tissue was fixed in 4% paraformaldehyde for at least 24 hrs and paraffin-embedded sections were prepared. Sections were stained with Haematoxylin-Eosin (H&E) to observe the pathological changes in the colon tissue. The histological index (HI) was determined concerning established standards as the sum of the three scores for the degree of inflammation, the site of inflammatory invasion and the degree of damage to the crypt structure[32].

The paraffin-embedded sections were dewaxed in xylene and dehydrated with gradient concentrations of alcohol. After antigen retrieval with EDTA, the Caspase-3 primary antibody (Abcam, Cambridge, Massachusetts, USA, product number GR89068-1) was added dropwise and the secondary antibody was added dropwise after incubation (4°C overnight). After DAB staining, dehydration, drying and sealing, the sections were observed under a microscope. Brown-yellow particles in the colon mucosa were defined as positive. Using the semi-quantitative analysis method, five fields of view were evaluated from each tissue section and the average IOD value for Caspase-3 protein expression in the mouse colon mucosa was detected using ImagePro Plus 6.0.

Table 1: Primers used for quantitative reverse transcription-polymerase chain reaction assay in this study

Name	GenBank accession		Sequence (5`-3`)	Product length (bp)
β-Actin	NM_007393.5	F	CATCCGTAAAGACCTCTATGCCAAC	171
		R	ATGGAGCCACCGATCCACA	
IL-6	NM_001314054.1	F	GGAGCCCACCAAGAACGATA	100
		R	TCACCAGCATCAGTCCCAAG	
TP53	NM_001127233.1	F	GGACCATCCTGGCTGTAGGTAG	144
		R	CGAGGCTGATATCCGACTGTGA	
Bax	NM_007527.3	F	CAGGATGCGTCCACCAAGAA	102
		R	CGTGTCCACGTCAGCAATCA	
Bcl2	NM_009741.5	F	CATTGTCGGGCCCATGAAG	168
		R	CACCCTGGCCCAATCTAGGA	
STAT3	NM_011486.5	F	CAGTGACTCAAAGCCACCTCATTC	127
		R	GGTGGTCAAGGCAAGCAGTTC	

IL-6: Interleukin-6, TP-53: Cellular tumour antigen p53, Bax: Apoptosis regulator BAX, Bcl2: Apoptosis regulator Bcl-2 and STAT3: Signal transducer and activator of transcription 3

Quantitative RT-PCR analysis: The RNAiso Plus and related reagents (TaKaRa, Kusatsu, Japan) were used to extract total RNA from the mouse colons. The PrimeScript RT Master Mix and related reagents were used for two-step reverse transcription to obtain complementary DNA. The TB Green Premix Ex Taq II and related reagents were used for real-time amplification and fluorescent signals were detected using the CFX96 Real-Time Polymerase Chain Reaction (PCR) Detection System. The expression levels of the target mRNAs interleukin (IL)-6, TP53, Bax, Bcl-2 and STAT3 were determined (Table 1). Using β-actin as an internal reference, the $2^{-\Delta\Delta ct}$ method was used to calculate the relative mRNA expression levels.

Detection of target protein expression in colon tissues by western blotting: Western blotting was used to validate the expression of IL-6 and TP53. Total protein was extracted from colon tissue using RIPA lysis buffer. The protein concentration was determined using the BCA method. The protein loading amount was calculated, followed by electrophoresis, membrane transfer, blocking and incubation with the primary antibodies for IL-6 (Abcam; Cat. No. GR4284-1) and TP53 (Abcam; Cat. No. GR56494-1) at 4°C overnight. Then, the membrane was washed and incubated with the secondary antibody (Boster Bio, Pleasanton, California, USA; Cat. No.: BA1050). Then the membrane was washed and scanned. A quantitative analysis of bands was performed using ImageJ. Optical density values were read. The relative expression levels of the target proteins are expressed as the grey value of the target protein/GAPDH.

Statistical analysis: Plots were generated and data were analysed using GraphPad Prism 9. After confirming normality and homogeneity of variances, data were compared by one-way analysis of variance. When the overall mean of each group was unequal or incomplete, the Bonferroni method was used for pairwise comparisons. The Kruskal-Wallis H test was used for comparative analysis when the variances were uneven or when the sample data did not meet the normality requirements. For unequal distributions, the Nemenyi method was used for pairwise comparisons. The $p<0.05$ was the threshold for significance and $p<0.01$ indicated a highly significant difference.

RESULTS

Candidate target identification: The molecular structure of the ART drug monomer was derived from the DrugBank database, as shown in Fig. 1a. The flowchart is as follows: go.drugbank.com/ Click on indications to enter→Select the disease you need→Get it indirectly through the target of the drug action Click on drug and targets→Click on target→Click on details under uniprot id→Select gene name (some may not). The chemical formula for the ART monomer was $C_{19}H_{28}O_8$, the relative molecular weight was 384.425, the melting point was 131-135°C. The structure contained 1 hydrogen bond donor and 7 hydrogen acceptors, the lipid-water partition coefficient (logPo/w) was 3.1 and the drug monomer complied with Lipinski's rule. A total of 154 potential ART targets (Fig. 1b) and 2,104 UC disease targets (Fig. 1c) were obtained.

PPI network construction and preliminary screening of ART targets in UC: The predicted ART targets were imported into the STRING database for PPI network construction and visualisation using Cytoscape (Fig. 2a). A PPI network of the key targets in UC was obtained following a similar method (Fig. 2b). After the intersection of ART key targets and UC targets, 29 common targets were obtained in the population (Fig. 2c), which were further imported into the STRING database for PPI network construction. The PPI network of potential targets of ART acting on UC was shown in Fig. 2d.

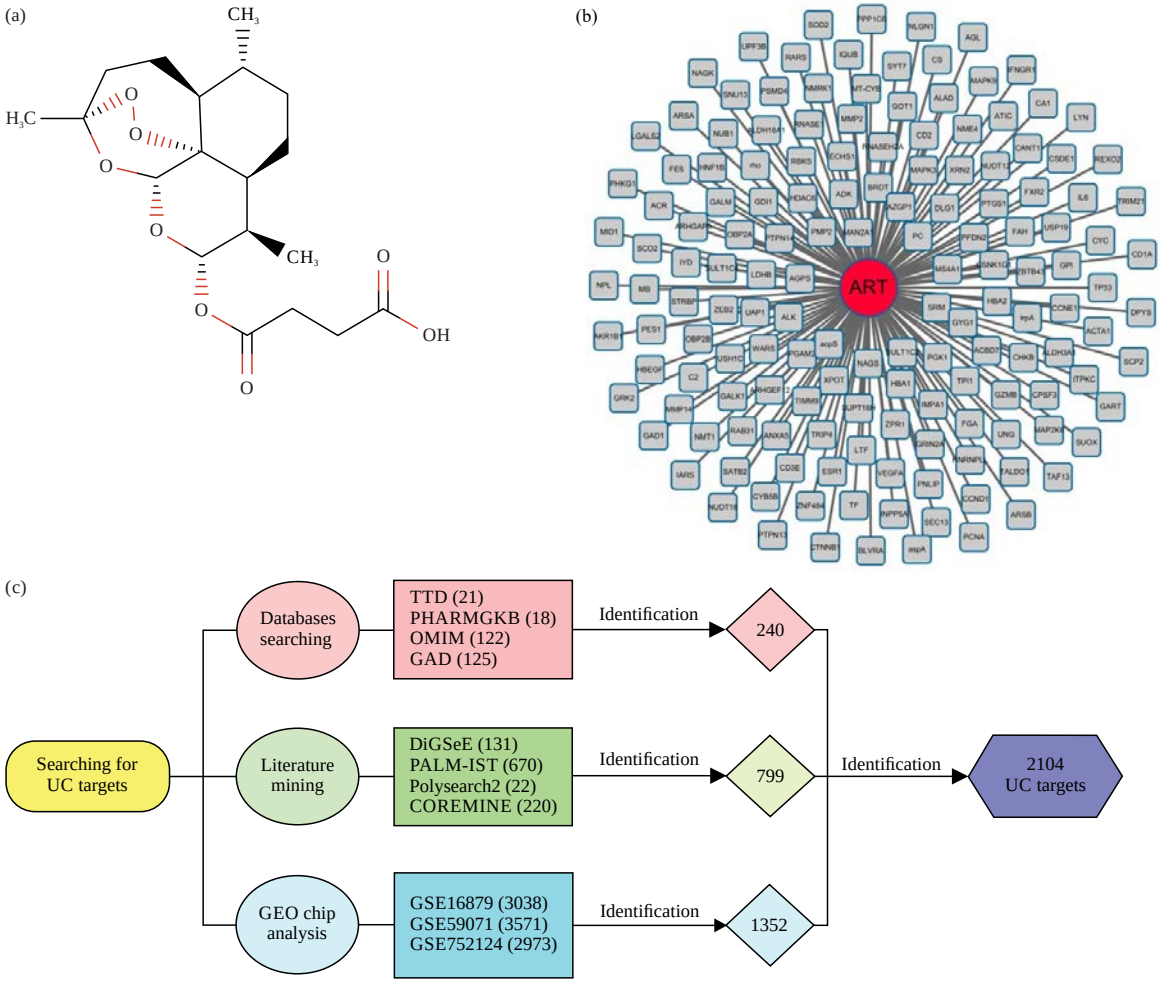

Fig. 1(a-c): Candidate target identification of ART and UC, (a) Chemical structure of ART and (b-c) A total of 154 potential ART targets and 2,104 UC disease targets were obtained

ART: Artesunate and UC: Ulcerative colitis

Gene ontology and KEGG pathway enrichment analyses: The GenCLiP database was used to perform a GO analysis of the 29 ART targets in UC. The analysis results obtained were shown in Fig. 3a. A total of 31 functional clusters and 96 GO terms were associated with the 29 targets. The gene functions included the regulation of the extracellular region, extracellular exosome, cell proliferation, apoptosis, small molecule metabolic process and immune system process.

The results obtained by the KEGG pathway enrichment analysis were summarised in Fig. 3b. A total of 21 of 29 targets were enriched in 11 pathway clusters and 39 pathways, including cancer-related signalling pathways, p53 signalling pathway, WNT signalling pathway and JAK/STAT signalling pathway.

Information for the potential targets of ART in the treatment of UC was further integrated with the results of the pathway enrichment analysis; after removing redundant signalling pathways identified in different databases, Cytoscape was used for the visualisation of an ART drug monomer-target-pathway network. Figure 3c displayed 1 ART drug monomer, 21 potential targets of ART enriched in pathways related to UC, 36 signalling pathway nodes and 113 branches.

Molecular docking analysis: In this experiment, 20 key targets corresponding to candidate ART targets in the PPI network were selected for validation via molecular docking to observe the binding activity. The crystalline structures and receptor information for the 20 targets included in the docking assay were shown in Fig. 4. The POCASA system was used to predict the active sites of the 20 protein receptors and information on the target receptor complexes used for docking was shown in

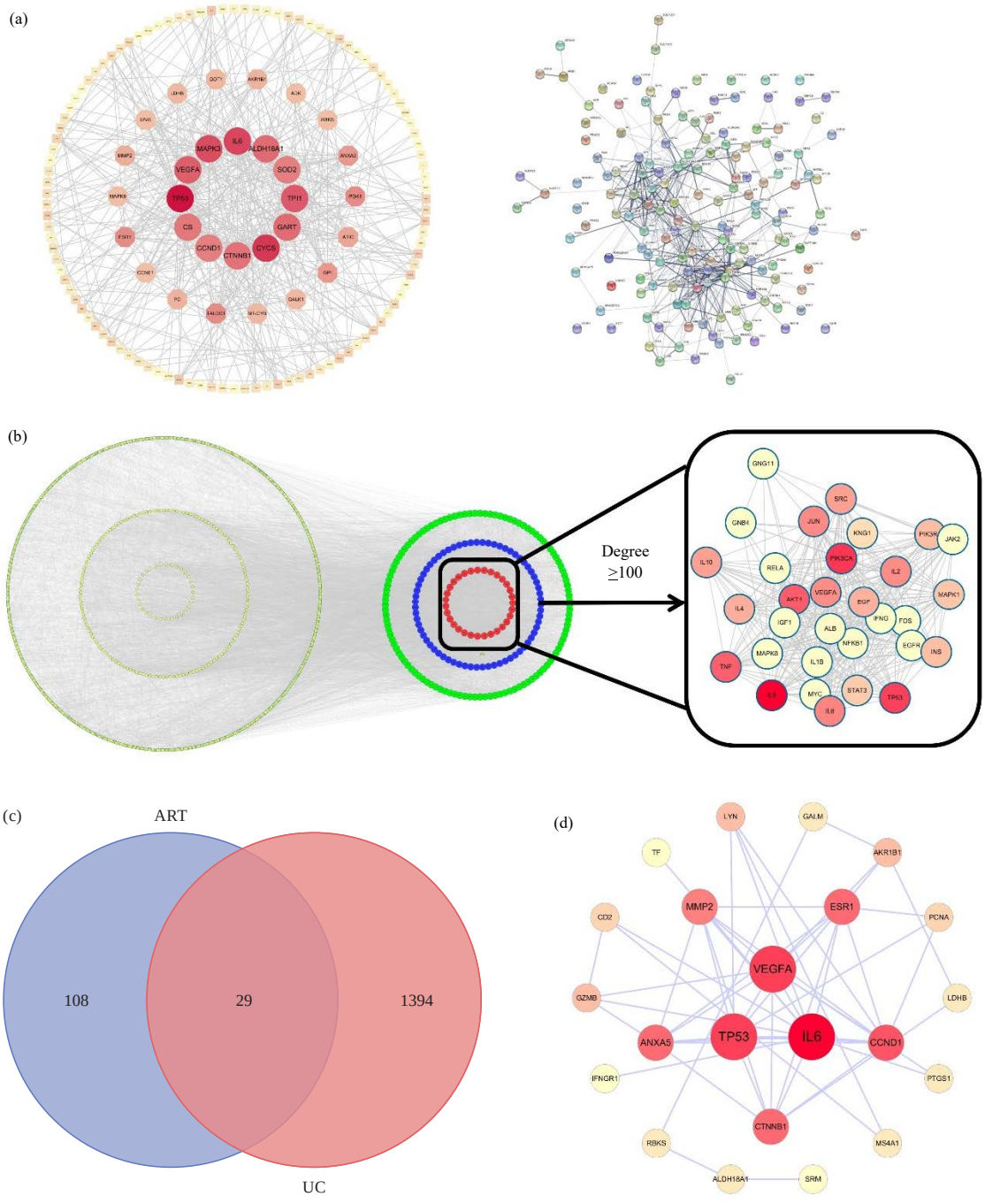

Fig. 2(a-d): PPI network construction and preliminary screening of ART targets in UC. Node colour is relative to its degree (the darker the colour, the greater the degree), (a) ART PPI network, (b) UC PPI network, (c) Intersection of UC targets and ART key targets and (d) PPI network of potential targets of ART acting on UC

(a) Comprised of 137 nodes and 462 edges, (b) Comprised of 1423 nodes and 13335 edges, (c) ART shares 29 putative targets with UC, (d) Network comprised of 22 nodes and 53 edges, ART: Artesunate, PPI: Protein-protein interaction and UC: Ulcerative colitis

Table S1. The ART monomer molecules were docked with the remaining receptors after removing the native ligands of the above 20 target proteins. The docking results were summarised in Table S2 and visualised in Fig. 5 and Fig. S1-20. The ART monomer molecules bound to 19 of the 20 targets screened by network pharmacology at the active site of the protein. The secondary docking results showed that the RMSD values of the 19 receptor-ligand complexes were all less than

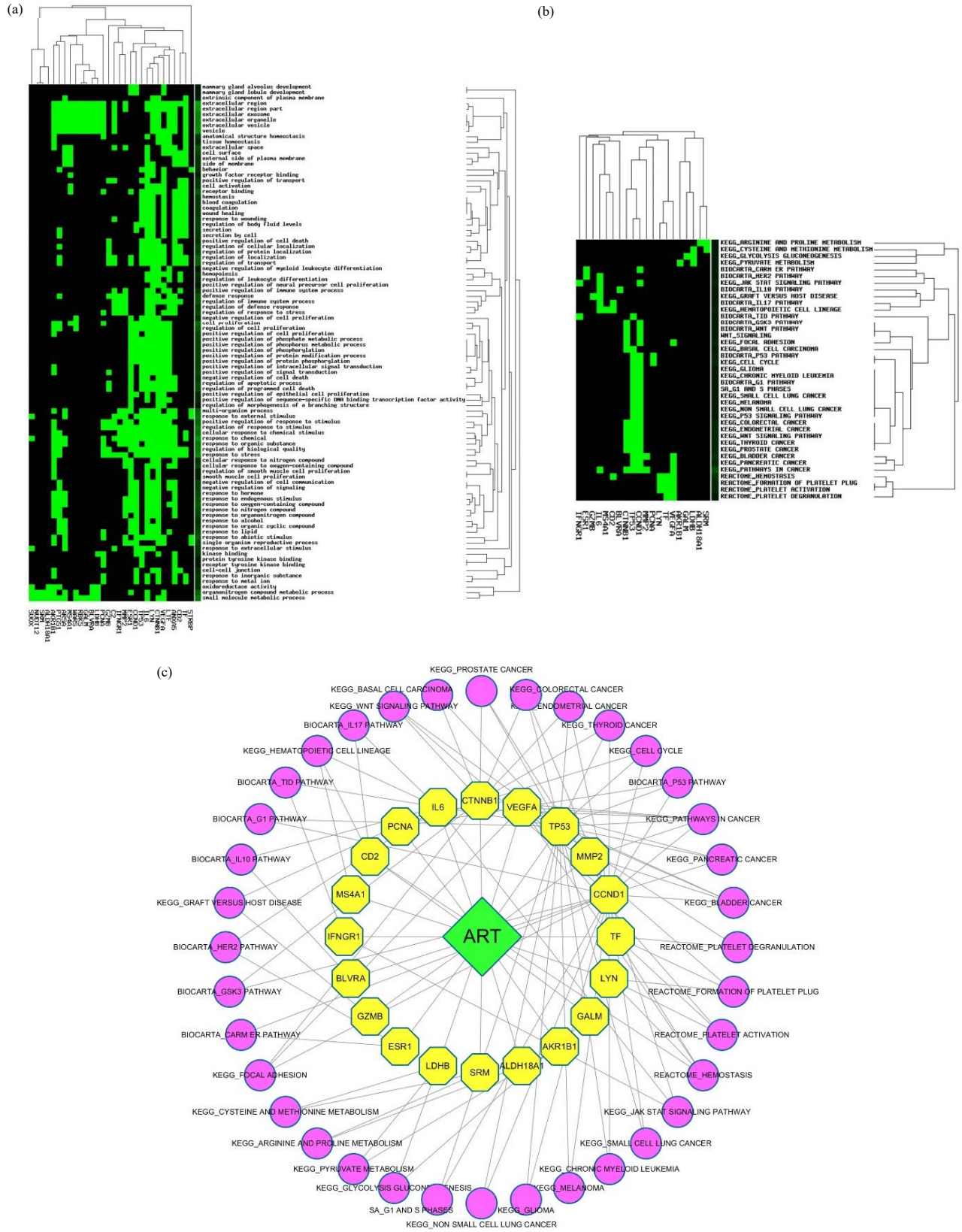

Fig. 3(a-c): Gene ontology and pathway enrichment analyses performed via GenCLiP, (a) GO enrichment analysis of target genes, (b) Signalling pathway enrichment of target genes and (c) Figure of signalling pathway-based drug targets

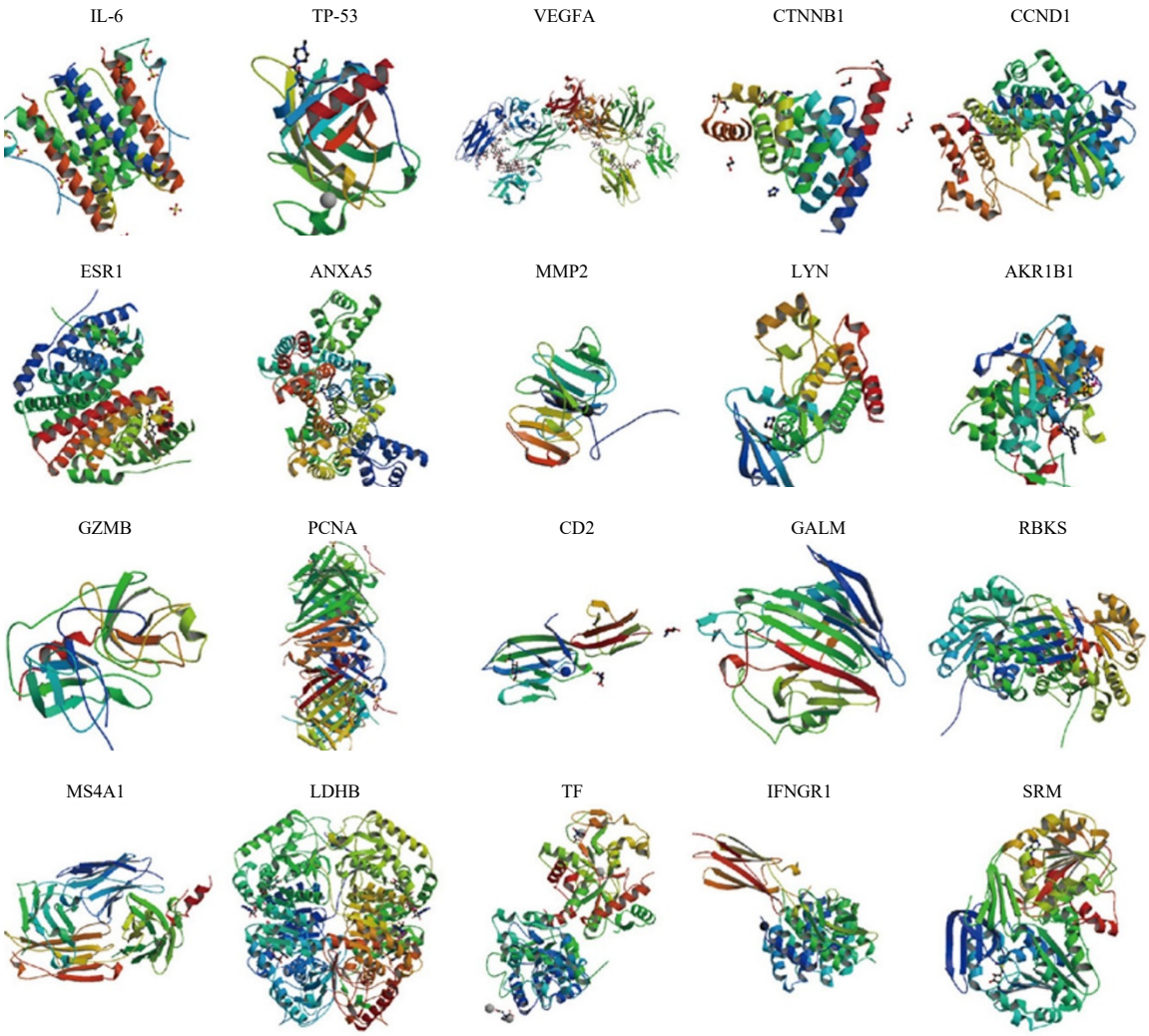

Fig. 4: Key target receptors corresponding to candidate ART targets in the PPI network
ART: Artesunate and PPI: Protein-protein interaction

2.0 Å, indicating that the docking results were accurate and reproducible. By a comparison of the docking results for ART on the 20 target protein receptors screened via network pharmacology, the active site could be complexed with the optimal conformational ligand-receptor complex of the pocket formed by successful docking. The top 5 target protein receptors with the lowest BE were AKR1B1, GZMB, TP53, IL-6 and LDHB and ART was likely to form stable interaction with the active sites of these receptors. Consolidating the network pharmacology-based screening results and ligand-receptor complexes obtained by molecular docking (Table 2), TP53 and IL-6 as two targets were selected for further validation (Fig. 6a-b).

ART effectively alleviated DSS-induced colonic inflammation in mice: The C57 mouse model of UC was successfully prepared by providing animals free access to 3% DSS. The mice in the model group differed significantly from those in the normal control group in terms of changes in body weight, colon length, DAI and pathological scores. After administration by intragastric gavage, ART effectively attenuated the 3% DSS-induced weight loss (Fig. 7a), shortened colon (Fig. 7b) and increased DAI and HI scores (Fig. 7c-d), among other disease symptoms and manifestations.

The H&E staining results of pathological sections (Fig. 7d) indicated that as compared to corresponding features in normal mice, the model group (3% DSS) showed more obvious lesions, including thickening of the intestinal wall, oedema of the lamina propria, necrosis or absence of colonic mucosal epithelial cells and infiltration of inflammatory cells and lymphocytes. Lesions were mainly detected in the mucosa and submucosa of the, the colonic crypt structure was destroyed, goblet cells were lost to varying degrees and

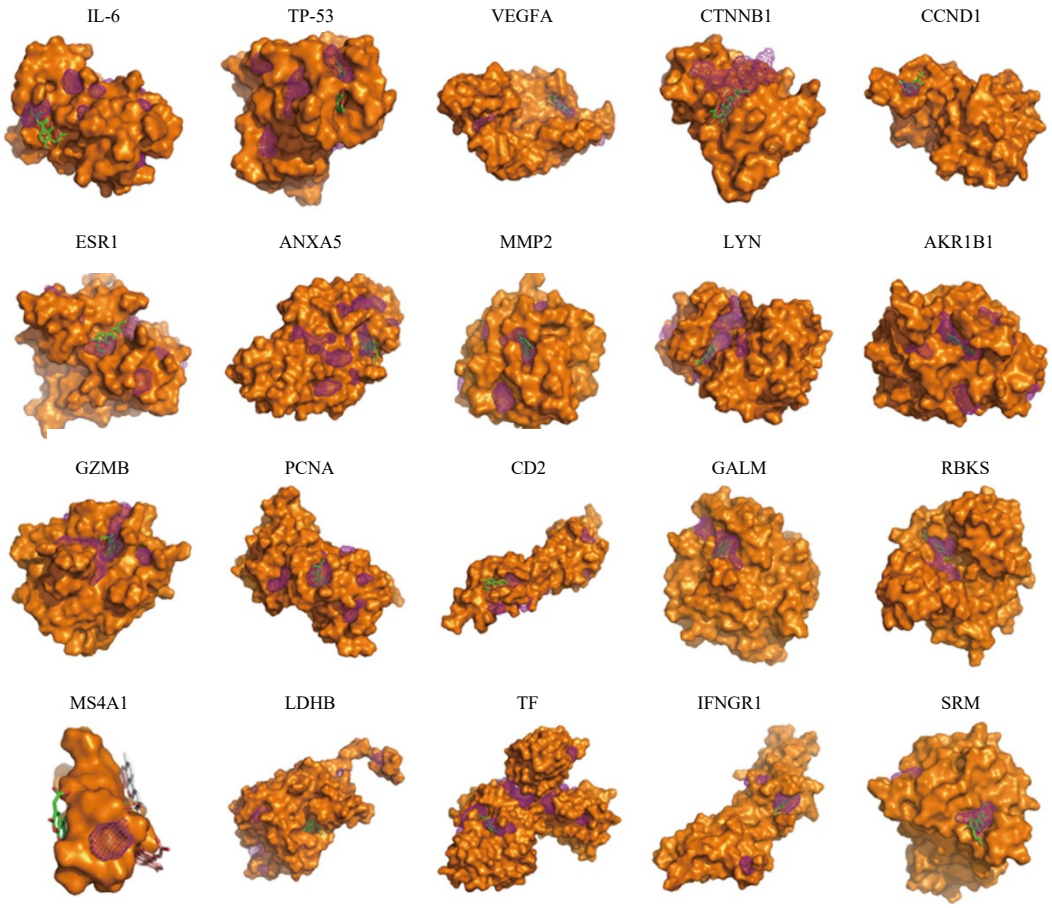

Fig. 5: Schematic illustration of the docking of ART with target proteins and purple meshes in the figure represent the active sites predicted by POCASA
ART: Artesunate

Table 2: Consolidation of PPI network and molecular docking analysis

Target	PDB ID	Binding energy of optimal docking conformer (kcal/mol)	Degrees of targets in the PPI network
IL6	1ALU	-10.74	13
TP53	5O1A	-11.27	10
VEGFA	5O4E	-9.15	10
AKR1B1	5OU0	-11.63	4
GZMB	4GAW	-11.52	4
MMP2	1RTG	-9.37	7
CCND1	2W96	-7.98	9
LDHB	1T2F	-10.68	2
LYN	5XY1	-8.61	4
ANXA5	1HAK	-7.75	8
CTNNB1	3SL9	-7.39	8
ESR1	2R6W	-7.16	8
CD2	1HNF	-8.1	3
GALM	1SNZ	-8.49	2
TF	5X5P	-9.7	1
RBKS	5BYC	-8.42	2
IFNGR1	1FYH	-8.73	1
PCNA	6HVO	-7.75	3
SRM	2O05	-8.54	1
MS4A1	2OSL	/	2

PPI: Protein-protein interaction

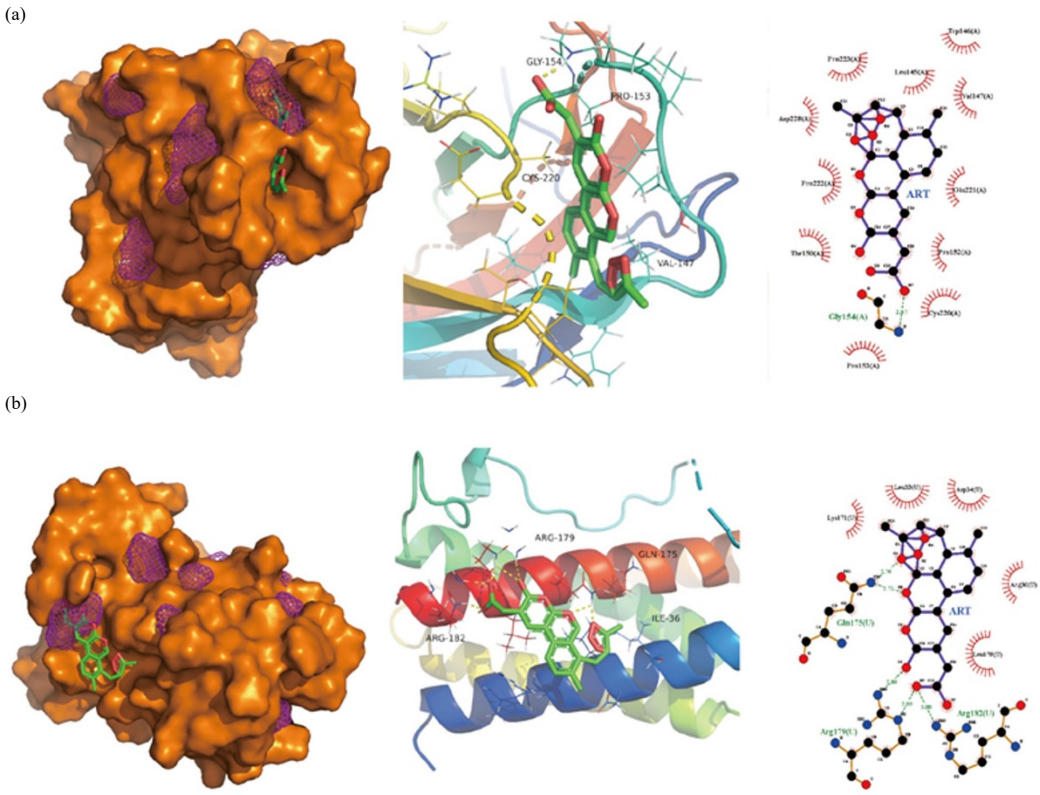

Fig. 6(a-b): Structural interactions of ART and key target receptors, (a) Docking results of ART on TP53 receptor (PDBID:5O1A) and (b) Docking results of ART on IL-6 receptor (PDBID:1ALU) and purple meshes in the figure represent the active sites predicted by POCASA
ART: Artesunate and IL-6: Interleukin-6

inflammatory cell infiltration was observed. In comparison with the structure in the model group, the colonic mucosal epithelial cells of mice in the ART group were more complete and the crypt structure and goblet cell structure were still partially preserved. These results indicated that the administration of ART could alleviate colonic tissue damage induced DSS in mice.

Effect of ART on TP53 and IL-6 expression in UC: As shown in Fig. 8, consolidating the mRNA and protein expression in colon tissues, in comparison with levels in the normal group, the expression levels of TP53 in the 3% DSS model group were significantly lower and the expression levels of IL-6 were significantly higher (Fig. 8a). After treatment with sulfasalazine and ART, the expression levels of TP53 in the colon tissues of mice were significantly higher than those in the model group and the expression levels of IL-6 were significantly lower (Fig. 8b).

Effect of ART on apoptosis in colon tissues of mice with UC: The RT-PCR analysis revealed that the levels of Bax mRNA expression in the model group were significantly less than in the normal group ($p<0.001$) (Fig. 9a). On the other hand, the levels of STAT3 and Bcl-2 mRNA expression were considerably greater in the model group compared to the normal group ($p<0.001$) (Fig. 9b). The study revealed a substantial decrease in the expression of Caspase-3 in the colon mucosa of mice in the UC model group compared to the control group ($p<0.001$).

These results suggested that the candidate targets may contribute to DSS-induced colon tissue damage and inflammation via the regulation of apoptosis. In comparison with levels in the model group, ART administration effectively increased the expression of Bax and Caspase-3 in the colons of mice and downregulate the expression of STAT3 and Bcl-2 ($p<0.001$).

DISCUSSION

The beneficial effects of ART in a DSS-induced enteritis mouse model have been previously demonstrated[7]; however, the mechanism underlying these effects remains unclear. In this study, potential targets of ART in UC were initially predicted using network pharmacology and molecular

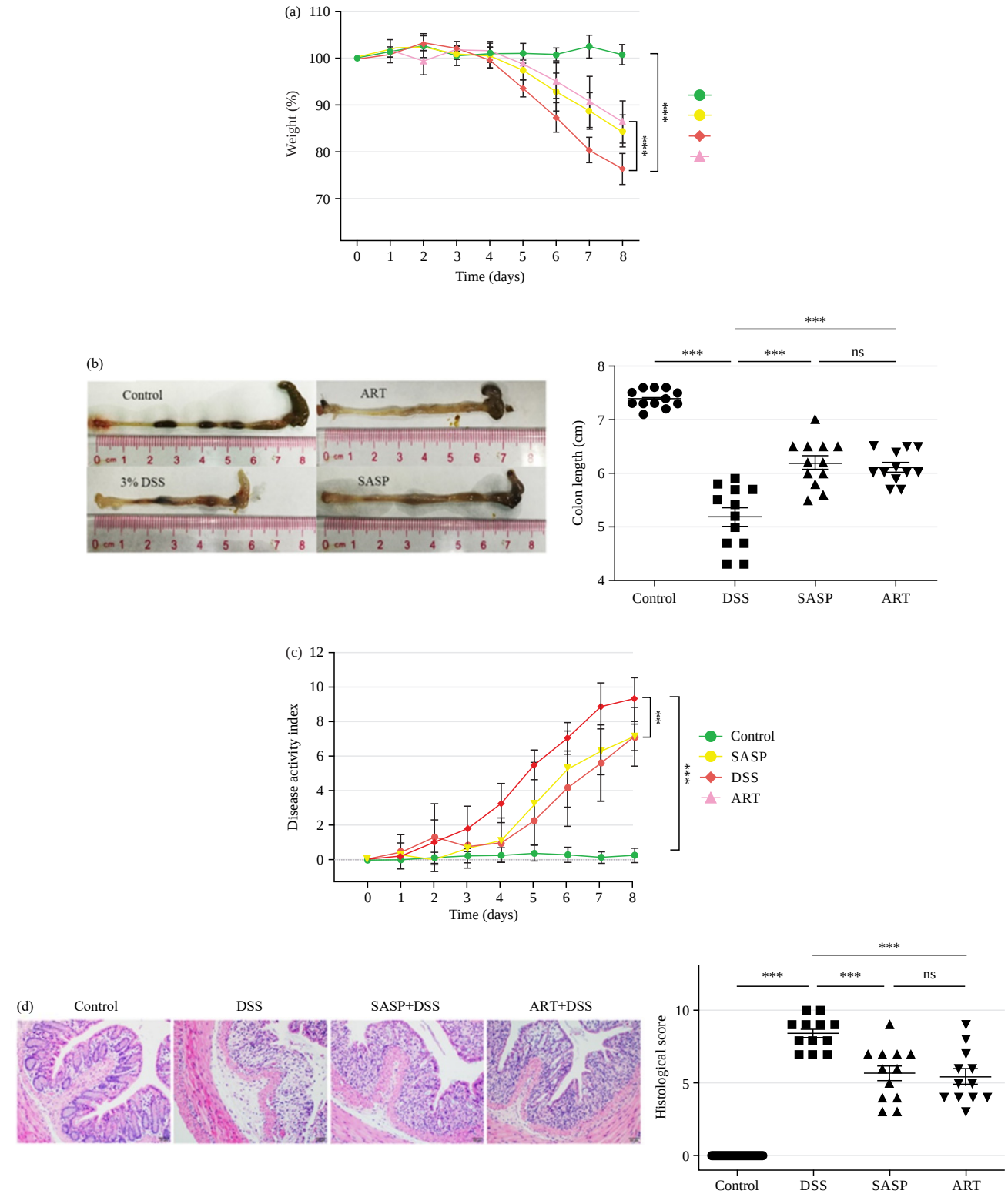

Fig. 7(a-d): ART effectively alleviated DSS-induced colonic inflammation in mice, (a) Body weight changes, (b) The macroscopic appearances (left) and length (right) of colon in different groups, (c) Disease activity index score and (d) H&E staining results of pathological sections (200× magnification) (left) and HI scores (right)

Data are presented as Mean±SEM (n = 12), *p<0.05, **p<0.01, ***p<0.001, ns: No significant differences, ART: Artesunate, DSS: Dextran sodium sulphate, H&E: Haematoxylin and Eosin, HI: Histological index and SEM: Standard error of the mean

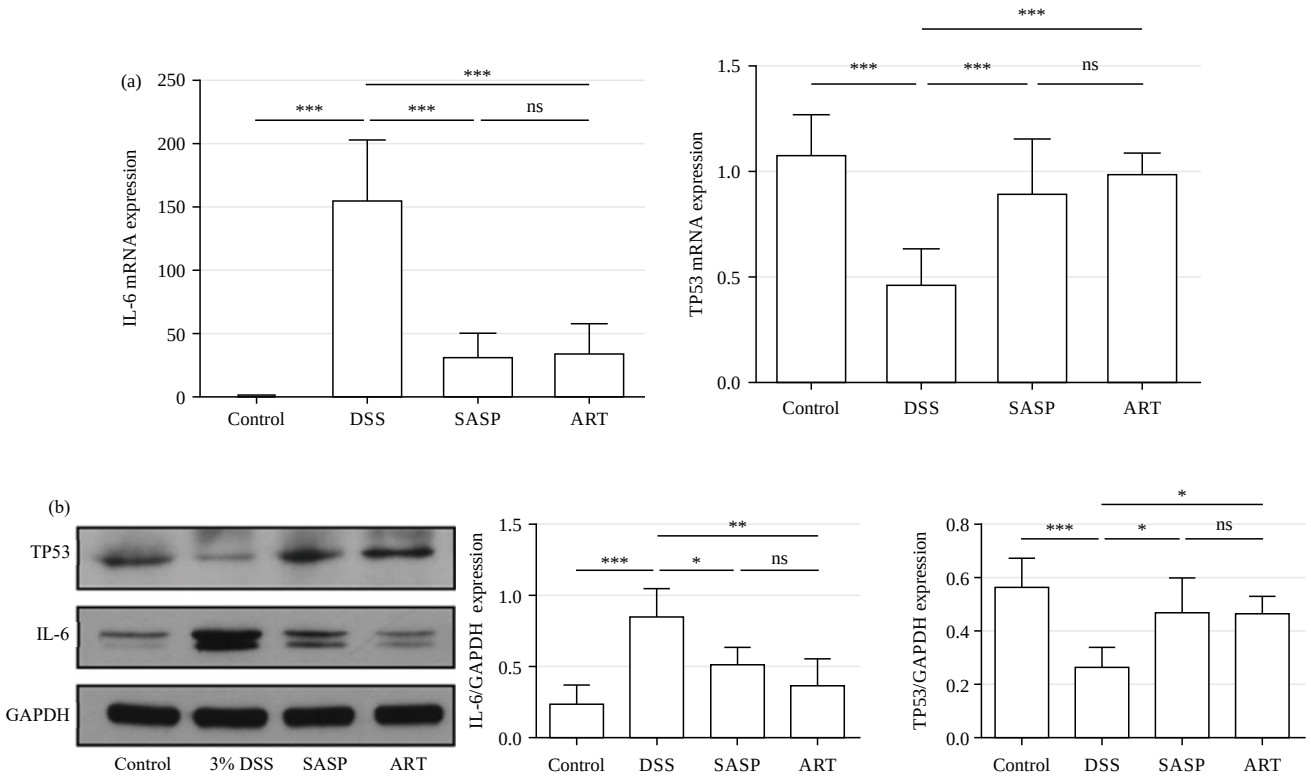

Fig. 8(a-b): Effect of ART on TP53 and IL-6 expression in UC, (a) Quantitative RT-PCR analysis was used to detect mRNA expression of IL-6 and TP53 in colon tissues (n = 12). β-actin was used as an internal reference and (b) Protein expression pf levels of TP53 and IL-6 in colon tissues were detected by western blotting (n = 6). The relative expression levels of TP53 and IL-6 proteins were quantified using densitometric analysis with GAPDH as internal control

Data are presented as Mean±SEM, *p<0.05, **p<0.01, ***p<0.001, ns: No significant differences, ART: Artesunate, IL-6: Interleukin-6, RT-PCR: Reverse-Transcription Polymerase Chain Reaction, GAPDH: Glyceraldehyde 3-Phosphate Dehydrogenase, SEM: Standard error of the mean and UC: Ulcerative colitis

docking. Targets with an important role in the PPI network (high-degree value) and good drug binding ability (as determined via BE) were identified for experimental verification. These analyses revealed various candidates, including IL-6, VEGFA, TP53, CCND1, ESR1, ANXA5 and other targets. In particular, IL-6 and TP53 were key candidates based on both the PPI network and molecular docking. Therefore, these two targets were first selected for validation.

The IL-6 is a pro-inflammatory cytokine produced by macrophages and secreted in the acute phase of inflammatory response; it is closely related to the pathogenesis of UC[33]. Elevated IL-6 mRNA expression has been found in the serum and tissue biopsies of patients with UC[34]. The IL-6 plays an important role in signal transduction by binding to its soluble receptor sIL-6R. The IL-6/sIL-6R complex can stimulate the expression of gp130 on the cell surface, leading to the activation of signal transducer and activator of transcription-3 (STAT3). The STAT3 is activated and translocated into the nucleus, promoting the transcription of target genes and the production of inflammatory factors[35]. In addition to the immune-inflammatory mechanism triggered by IL-6, studies have shown that STAT3 can induce the expression of the anti-apoptotic factors Bcl-2 and Bcl-xl, thereby reducing T cell apoptosis, which in turn leads to T cell aggregation and the induction of chronic intestinal inflammation[36].

The TP53 (transcription factor p53) is a target gene that can regulate or induce cell cycle arrest, apoptosis and senescence as well as DNA repair and metabolic changes by acting on various cellular stress responses[37]. Studies have shown that TP53 can control and reduce the production and upregulation of inflammatory cytokines by initiating related cellular senescence programs[38]. Yamanishi *et al.*[39] found that in the synovial tissue of patients with rheumatoid arthritis, regions with a higher TP53 mutation rate showed higher IL-6 mRNA levels, indicating that cells with reduced expression and decreased regulatory function due to TP53 mutations will

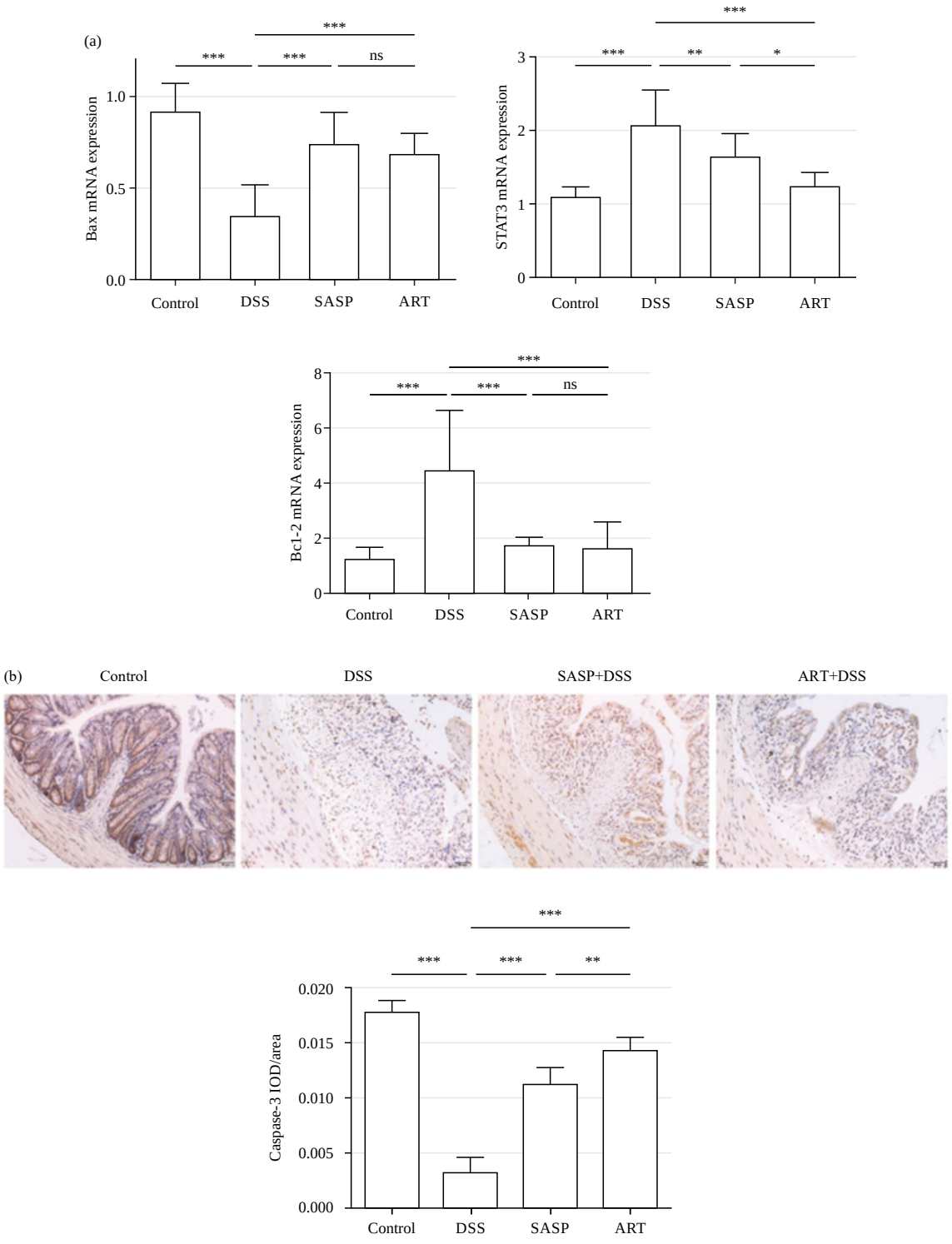

Fig. 9(a-d): Effect of ART on apoptosis in colon tissues of mice with UC, (a) mRNA expression of Bax, STAT3 and Bcl-2 in colon tissues were detected via quantitative RT-PCR analysis (n = 12). β-actin was used as an internal reference and (b) Immunohistochemical staining images of each group for Caspase-3 (200× magnification) and average IOD value for Caspase-3 protein expression in mice's colon mucosa

Data are presented as Mean±SEM, *p<0.05, **p<0.01, ***p<0.001, ns: No significant differences, ART: Artesunate, RT-PCR: Reverse-Transcription Polymerase Chain Reaction, SEM: Standard error of the mean and UC: Ulcerative colitis

aggravate inflammation by upregulating inflammatory factors, such as IL-6, in adjacent cells. The deletion of TP53 can lead to the accumulation of damaged intestinal epithelial cells in mice and affect the regeneration of epithelial cells, which in turn leads to the occurrence of local inflammation and increased mortality in mice[40]. Clinical studies have shown that the expression level of TP53 in the peripheral blood of patients with UC is significantly lower than that in healthy adults[41]. In addition, experiments have shown that ART could have therapeutic effects in some diseases by targeting TP53[42,43]; for example, ART could increase the expression of p53 at the protein and mRNA levels in hepatic stellate cells, conferring anti-hepatic fibrosis effects[44].

Current study results revealed the expression of IL-6 was significantly higher and TP53 was significantly lower in the model group than in the normal group. The ART effectively reduced the expression of IL-6 in the colon of mice and increased the expression of TP53. A GO analysis indicated that potential targets screened by network pharmacology were involved in cancer-related pathways, the P53 pathway and JAK/STAT signalling pathways, demonstrating a clear link to apoptosis. Many previous studies have shown that apoptosis is closely related to the pathogenesis of inflammatory bowel disease[45-48]; accordingly, in this study, expression analyses focused on apoptosis-related factors Bax, Bcl-2, STAT3 and Caspase-3 were performed.

The Bax and Bcl-2 are members of the Bcl-2 gene family and are downstream factors in the p53 signalling pathway. The Bcl-2 family plays a central role in the apoptosis pathway[49], in which Bcl-2 has inhibitory effects on apoptosis, while Bax can antagonise the inhibitory effect of Bcl-2 and is classified as a pro-apoptotic gene. The expression of Bax can enhance mitochondrial permeability, leading to the release of cytochrome c, which in turn leads to the activation of the Caspase family, including Caspase-9 and Caspase-3, leading to apoptosis[50]. Reinecke *et al.*[45] found that UC is associated with an increase in the expression of Bcl-2 in inflammatory cells, leading to the inhibition of apoptosis in inflammatory cells, which in turn leads to the infiltration of many inflammatory cells in the intestinal mucosa of patients with active UC and the continuous activation of inflammation. Other studies have shown that the apoptosis of colonic mucosal lymphocytes is blocked and its cytotoxic effect contributes to inflammation in UC; the inhibition of apoptosis is closely related to the overexpression of Bcl-2 and the decreased expression of the downstream factor Caspase-3 in the p53 signalling pathway[51]. These findings indicate that the TP53 gene and its related apoptosis signalling pathway are closely related to the pathogenesis of inflammation-immunity and may be an important target in the pathogenesis of UC. Studies have shown that ART can induce apoptosis in HepG2, Huh-7 and Hep3B liver carcinoma cells via Bax-mediated apoptosis[51,52]. In addition, ART can increase the expression of Bax and Caspase-3 in HCT116 colon cancer cells, reduce the protein expression levels of Bcl-2 and Bcl-xL and then induce apoptosis and autophagy[53]. These results supported the therapeutic value of ART in precancerous lesions of UC via the apoptotic pathway.

In this study, Bax mRNA expression in the UC model group was significantly lower than that in the normal group, while Bcl-2 mRNA expression was significantly higher in the model group than in the normal group. The expression of Caspase-3 decreased in the colonic mucosa of the mice, suggesting that Bax/Bcl-2-Caspase-3, an apoptotic signalling process, plays a key role in DSS-induced colon tissue damage and inflammation in mice. In addition, the expression of STAT3 mRNA in the model group was significantly increased. In combination with previous results of Mudter and Neurath[36], these findings suggested that apoptosis accelerated the intestinal inflammation process in the model group via a reduction in T cell apoptosis, which in turn led to the accumulation of T cells and increased intestinal inflammation. In comparison with levels in the model group, ART can effectively increase the expression of TP53 and Bax mRNA in the mouse colon and downregulate the expression of STAT3 and Bcl-2 mRNA, resulting in a decrease in the expression of the downstream protein Caspase-3, suggesting that ART may regulate Caspase-3 expression in the colon. This signalling pathway increased the apoptosis of inflammatory cells, reduced the cytotoxic effect and ameliorated DSS-induced colon tissue damage and inflammation in mice.

There are also limitations of this study. First, only two candidate targets screened via network pharmacology and molecular docking approaches were evaluated and the validation of other targets is required. As such, further studies are needed to explore the specific mechanism by which ART alleviates UC via the apoptotic pathway.

CONCLUSION

By using network pharmacology and molecular docking, potential targets and mechanisms of artesunate in the treatment of ulcerative colitis were identified. Further, *in vivo* experiments showed that artesunate can effectively alleviate inflammation and injury in the mouse colon after treatment with 3% dextran sodium sulphate. These effects might be mediated by TP53 and interleukin-6 and their regulation of apoptosis and inflammation. Our findings may provide new insights into the discovery of new drugs for ulcerative colitis treatment.

SIGNIFICANCE STATEMENT

This research used network pharmacology, molecular docking and animal trials to predict artesunate targets, processes and ulcerative colitis efficacy. Network pharmacology and molecular docking discovered artesunate's ulcerative colitis targets and processes. *In vivo*, tests indicated that artesunate reduces mouse colon inflammation and damage following 3% dextran sodium sulphate therapy. The TP53 and interleukin-6 may regulate apoptosis and inflammation to cause these effects. These discoveries may help develop novel ulcerative colitis medicines.

ACKNOWLEDGMENT

The authors acknowledge the services offered by higher authorities.

REFERENCES

1. Burrows, J.N., K. Chibale and T.N.C. Wells, 2011. The state of the art in anti-malarial drug discovery and development. Curr. Top. Med. Chem., 11: 1226-1254.
2. Xu, Z., X. Liu and D. Zhuang, 2022. Artesunate inhibits proliferation, migration, and invasion of thyroid cancer cells by regulating the PI3K/AKT/FKHR pathway. Biochem. Cell Biol., 100: 85-92.
3. Li, B., Z. Zhang and Y. Fu, 2021. Anti-inflammatory effects of artesunate on atherosclerosis via miR-16-5p and TXNIP regulation of the NLRP3 inflammasome. Ann. Transl. Med., Vol. 9. 10.21037/atm-21-4939.
4. Hou, L. and H. Huang, 2016. Immune suppressive properties of artemisinin family drugs. Pharmacol. Ther., 166: 123-127.
5. Yang, Z., J. Ding, C. Yang, Y. Gao and X. Li *et al*., 2012. Immunomodulatory and anti-inflammatory properties of artesunate in experimental colitis. Curr. Med. Chem., 19: 4541-4551.
6. Zhang, R., X. Zhu, H. Bai and K. Ning, 2019. Network pharmacology databases for traditional Chinese medicine: Review and assessment. Front. Pharmacol., Vol. 10. 10.3389/fphar.2019.00123.
7. Mendez, D., A. Gaulton, A.P. Bento, J. Chambers and M. de Veij *et al*., 2019. ChEMBL: Towards direct deposition of bioassay data. Nucleic Acids Res., 47: D930-D940.
8. Daina, A., O. Michielin and V. Zoete, 2019. SwissTargetPrediction: Updated data and new features for efficient prediction of protein targets of small molecules. Nucleic Acids Res., 47: W357-W364.
9. Nickel, J., B.O. Gohlke, J. Erehman, P. Banerjee and W.W. Rong *et al*., 2014. SuperPred: Update on drug classification and target prediction. Nucleic Acids Res., 42: W26-W31.
10. Wang, X., Y. Shen, S. Wang, S. Li and W. Zhang *et al*., 2017. PharmMapper 2017 update: A web server for potential drug target identification with a comprehensive target pharmacophore database. Nucleic Acids Res., 45: W356-W360.
11. The UniProt Consortium, 2021. UniProt: The universal protein knowledgebase in 2021. Nucleic Acids Res., 49: D480-D489.
12. Zhou, Y., Y. Zhang, X. Lian, F. Li and C. Wang *et al*., 2022. Therapeutic target database update 2022: Facilitating drug discovery with enriched comparative data of targeted agents. Nucleic Acids Res., 50: D1398-D1407.
13. Whirl-Carrillo, M., R. Huddart, L. Gong, K. Sangkuhl, C.F. Thorn, R. Whaley and T.E. Klein, 2021. An evidence-based framework for evaluating pharmacogenomics knowledge for personalized medicine. Clin. Pharmacol. Ther., 110: 563-572.
14. Amberger, J.S., C.A. Bocchini, A.F. Scott and A. Hamosh, 2019. OMIM.org: Leveraging knowledge across phenotype-gene relationships. Nucleic Acids Res., 47: D1038-D1043.
15. Becker, K.G., K.C. Barnes, T.J. Bright and S.A. Wang, 2004. The genetic association database. Nat. Genet., 36: 431-432.
16. Kim, J., S. So, H.J. Lee, J.C. Park, J.J. Kim and H. Lee, 2013. DigSee: Disease gene search engine with evidence sentences (version cancer). Nucleic Acids Res., 41: W510-W517.
17. Mandloi, S. and S. Chakrabarti, 2015. PALM-IST: Pathway assembly from literature mining-an information search tool. Sci. Rep., Vol. 5. 10.1038/srep10021.
18. Liu, Y., Y. Liang and D. Wishart, 2015. PolySearch2: A significantly improved text-mining system for discovering associations between human diseases, genes, drugs, metabolites, toxins and more. Nucleic Acids Res., 43: W535-W542.
19. de Leeuw, N., T. Dijkhuizen, J.Y. Hehir-Kwa, N.P. Carter and L. Feuk *et al*., 2012. Diagnostic interpretation of array data using public databases and internet sources. Hum. Mutat., 33: 930-940.
20. Szklarczyk, D., A.L. Gable, D. Lyon, A. Junge and S. Wyder *et al*., 2019. String v11: Protein-protein association networks with increased coverage, supporting functional discovery in genome-wide experimental datasets. Nucleic Acids Res., 47: D607-D613.
21. Shannon, P., A. Markiel, O. Ozier, N.S. Baliga and J.T. Wang *et al*., 2003. Cytoscape: A software environment for integrated models of biomolecular interaction networks. Genome Res., 13: 2498-2504.
22. Wang, J.H., L.F. Zhao, H.F. Wang, Y.T. Wen and K.K. Jiang *et al*., 2020. GenCLiP 3: Mining human genes' functions and regulatory networks from PubMed based on co-occurrences and natural language processing. Bioinformatics, 36: 1973-1975.

23. Wishart, D.S., Y.D. Feunang, A.C. Guo, E.J. Lo and A. Marcu *et al*., 2018. DrugBank 5.0: A major update to the DrugBank database for 2018. Nucleic Acids Res., 46: D1074-D1082.
24. Berman, H.M., J. Westbrook, Z. Feng, G. Gilliland and T.N. Bhat *et al*., 2000. The protein data bank. Nucleic Acids Res., 28: 235-242.
25. Yu, J., Y. Zhou, I. Tanaka and M. Yao, 2010. Roll: A new algorithm for the detection of protein pockets and cavities with a rolling probe sphere. Bioinformatics, 26: 46-52.
26. Morris, G.M., R. Huey, W. Lindstrom, M.F. Sanner, R.K. Belew, D.S. Goodsell and A.J. Olson, 2009. AutoDock4 and AutoDock Tools4: Automated docking with selective receptor flexibility. J. Comput. Chem., 30: 2785-2791.
27. Laskowski, R.A. and M.B. Swindells, 2011. LigPlot+: Multiple ligand-protein interaction diagrams for drug discovery. J. Chem. Inf. Model., 51: 2778-2786.
28. Nunes, N.S., S. Kim, M. Sundby, P. Chandran, S.R. Burks, A.H. Paz and J.A. Frank, 2018. Temporal clinical, proteomic, histological and cellular immune responses of dextran sulfate sodium-induced acute colitis. World J. Gastroenterol., 24: 4341-4355.
29. Xiao, H.T., C.Y. Lin, D.H.H. Ho, J. Peng and Y. Chen *et al*., 2013. Inhibitory effect of the *Gallotannin corilagin* on dextran sulfate sodium-induced murine ulcerative colitis. J. Nat. Prod., 76: 2120-2125.
30. Mi, H., F.B. Liu, H.W. Li, J.T. Hou and P.W. Li, 2017. Anti-inflammatory effect of Chang-An-Shuan on TNBS-induced experimental colitis in rats. BMC Complementary Altern. Med., Vol. 17. 10.1186/s12906-017-1794-0.
31. Wen, S., Z. Zhong, L. He, D. Zhao, X. Chen, H. Mi and F. Liu, 2021. Network pharmacology dissection of multiscale mechanisms for Jiaoqi powder in treating ulcerative colitis. J. Ethnopharmacol., Vol. 275. 10.1016/j.jep.2021.114109.
32. Andújar, I., M.C. Recio, R.M. Giner, E. Cienfuegos-Jovellanos, S. Laghi, B. Muguerza and J.L. Ríos, 2011. Inhibition of ulcerative colitis in mice after oral administration of a polyphenol-enriched cocoa extract is mediated by the inhibition of STAT1 and STAT3 phosphorylation in colon cells. J. Agric. Food Chem., 59: 6474-6483.
33. Mudter, J. and M.F. Neurath, 2007. Il-6 signaling in inflammatory bowel disease: Pathophysiological role and clinical relevance. Inflammatory Bowel Dis., 13: 1016-1023.
34. Reimund, J.M., C. Wittersheim, S. Dumont, C.D. Muller, R. Baumann, P. Poindron and B. Duclos, 1996. Mucosal inflammatory cytokine production by intestinal biopsies in patients with ulcerative colitis and Crohn's disease. J. Clin. Immunol., 16: 144-150.
35. Kallen, K.J., 2002. The role of transsignalling via the agonistic soluble IL-6 receptor in human diseases. Biochim. Biophys. Acta Mol. Cell Res., 1592: 323-343.
36. Mudter, J. and M.F. Neurath, 2007. Apoptosis of T cells and the control of inflammatory bowel disease: Therapeutic implications. Gut, 56: 293-303.
37. Vousden, K.H. and D.P. Lane, 2007. p53 in health and disease. Nat. Rev. Mol. Cell Biol., 8: 275-283.
38. Xue, W., L. Zender, C. Miething, R.A. Dickins and E. Hernando *et al*., 2007. Senescence and tumour clearance is triggered by p53 restoration in murine liver carcinomas. Nature, 445: 656-660.
39. Yamanishi, Y., D.L. Boyle, S. Rosengren, D.R. Green, N.J. Zvaifler and G.S. Firestein, 2002. Regional analysis of *p53* mutations in rheumatoid arthritis synovium. Proc. Natl. Acad. Sci. USA, 99: 10025-10030.
40. Ruzankina, Y., D.W. Schoppy, A. Asare, C.E. Clark, R.H. Vonderheide and E.J. Brown, 2009. Tissue regenerative delays and synthetic lethality in adult mice after combined deletion of *Atr* and *Trp53*. Nat. Genet., 41: 1144-1149.
41. Su, H., Q. Kang, H. Wang, H. Yin, L. Duan, Y. Liu and R. Fan, 2019. Changes in expression of p53 and inflammatory factors in patients with ulcerative colitis. Exp. Ther. Med., 17: 2451-2456.
42. Wang, Z., Q. Wang, T. He, W. Li and Y. Liu *et al*., 2020. The combination of artesunate and carboplatin exerts a synergistic anti-tumour effect on non-small cell lung cancer. Clin. Exp. Pharmacol. Physiol., 47: 1083-1091.
43. Wan, Q., H. Chen, X. Li, L. Yan, Y. Sun and J. Wang, 2019. Artesunate inhibits fibroblasts proliferation and reduces surgery-induced epidural fibrosis via the autophagy-mediated p53/p21$^{waf1/cip1}$ pathway. Eur. J. Pharmacol., 842: 197-207.
44. Longxi, P., F. Buwu, W. Yuan and G. Sinan, 2011. Expression of p53 in the effects of artesunate on induction of apoptosis and inhibition of proliferation in rat primary hepatic stellate cells. PLoS ONE, Vol. 6. 10.1371/journal.pone.0026500.
45. Reinecke, K., S. Eminel, F. Dierck, W. Roessner and S. Kersting *et al*., 2012. The JNK inhibitor XG-102 protects against TNBS-induced colitis. PLoS ONE, Vol. 7. 10.1371/journal.pone.0030985.
46. Chen, X., M. Li, D. Li, T. Luo and Y. Xie *et al*., 2020. Ethanol extract of *Pycnoporus sanguineus* relieves the dextran sulfate sodium-induced experimental colitis by suppressing helper T cell-mediated inflammation via apoptosis induction. Biomed. Pharmacother., Vol. 127. 10.1016/j.biopha.2020.110212.
47. Zhou, Y., F. Dou, H. Song and T. Liu, 2022. Anti-ulcerative effects of wogonin on ulcerative colitis induced by dextran sulfate sodium via Nrf2/TLR4/NF-κB signaling pathway in BALB/c mice. Environ. Toxicol., 37: 954-963.

48. Leal, R.F., M. de Lourdes S Ayrizono, M. Milanski, J.J. Fagundes and J.C. Moraes *et al*., 2010. Detection of epithelial apoptosis in pelvic ileal pouches for ulcerative colitis and familial adenomatous polyposis. J. Transl. Med., Vol. 8. 10.1186/1479-5876-8-11.
49. Solano-Gálvez, S.G., J. Abadi-Chiriti, L. Gutiérrez-Velez, E. Rodríguez-Puente and E. Konstat-Korzenny *et al*., 2018. Apoptosis: Activation and inhibition in health and disease. Med. Sci., Vol. 6. 10.3390/medsci 6030054.
50. Martinou, J.C. and R.J. Youle, 2011. Mitochondria in apoptosis: Bcl-2 family members and mitochondrial dynamics. Dev. Cell, 21: 92-101.
51. Liu, C., Y. Zeng, Y. Wen, X. Huang and Y. Liu, 2022. Natural products modulate cell apoptosis: A promising way for the treatment of ulcerative colitis. Front. Pharmacol., Vol. 13. 10.3389/fphar.2022.806148.
52. Pang, Y., G. Qin, L. Wu, X. Wang and T. Chen, 2016. Artesunate induces ROS-dependent apoptosis via a Bax-mediated intrinsic pathway in Huh-7 and Hep3B cells. Exp. Cell Res., 347: 251-260.
53. Jiang, F., J.Y. Zhou, D. Zhang, M.H. Liu and Y.G. Chen, 2018. Artesunate induces apoptosis and autophagy in HCT116 colon cancer cells, and autophagy inhibition enhances the artesunate-induced apoptosis. Int. J. Mol. Med., 42: 1295-1304.

SUPPLEMENTARY DATA

Table S1: Information on the target receptor complexes used for docking

Gene names	PDB ID	Chain ID	Number of active site
Interleukin-6 (IL6)	1ALU	A	9
Transcription factor p53 (TP53)	5O1A	A	6
Vascular endothelial growth factor A (VEGFA)	5O4E	E	5
Catenin beta-1 (CTNNB1)	3SL9	A	8
G1/S-specific cyclin-D1 (CCND1)	2W96	A	4
Estrogen receptor (ESR1)	2R6W	A	9
Annexin A5 (ANXA5)	1HAK	B	14
Human gelatinase A (MMP2)	1RTG	A	6
Tyrosine-protein kinase Lyn (LYN)	5XY1	A	6
Aldose reductase (AKR1B1)	5OU0	A	8
Granzyme H (GZMB)	4GAW	D	7
Proliferating cell nuclear antigen (PCNA)	6HVO	A	7
T-cell surface antigen CD2 (CD2)	1HNF	A	9
Aldose 1-epimerase (GALM)	1SNZ	A	7
Ribokinase (RBKS)	5BYC	A	5
B-lymphocyte antigen CD20 (MS4A1)	2OSL	P	1
L-lactate dehydrogenase B chain (LDHB)	1T2F	B	16
Serotransferrin (TF)	5X5P	A	15
Interferon gamma (IFNGR1)	1FYH	B	4
Spermidine synthase (SRM)	2O05	A	6

Table S2: Docking results of proteins

Target protein	PDB ID	Binding at active site	Binding energy of optimal docking conformer (kcal/mol)	RMSD values of secondary docking Å
AKR1B1	5OU0	yes	-11.63	0.34
GZMB	4GAW	yes	-11.52	0.34
TP53	5O1A	yes	-11.27	0.20
IL6	1ALU	yes	-10.74	0.37
LDHB	1T2F	yes	-10.68	0.83
TF	5X5P	yes	-9.7	1.77
MMP2	1RTG	yes	-9.37	1.85
VEGFA	5O4E	yes	-9.15	0.58
IFNGR1	1FYH	yes	-8.73	1.82
LYN	5XY1	yes	-8.61	0.77
SRM	2O05	yes	-8.54	1.63
GALM	1SNZ	yes	-8.49	1.46
RBKS	5BYC	yes	-8.42	0.36
CD2	1HNF	yes	-8.1	0.60
CCND1	2W96	yes	-7.98	1.29
ANXA5	1HAK	yes	-7.75	1.58
PCNA	6HVO	yes	-7.75	1.30
CTNNB1	3SL9	yes	-7.39	0.91
ESR1	2R6W	yes	-7.16	0.80
MS4A1	2OSL	no	/	/

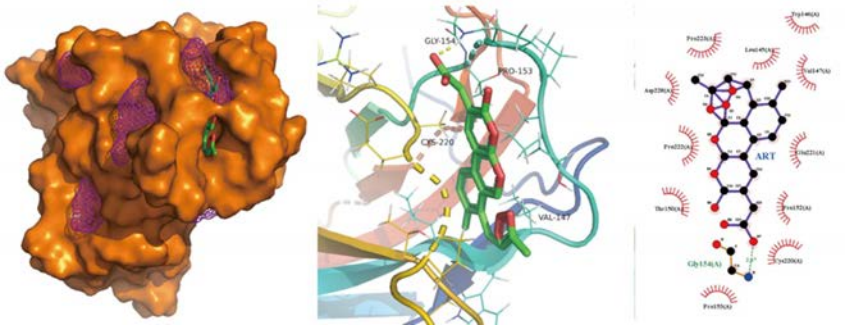

Fig. S1: Docking results of ART monomer molecule and TP53 protein (5O1A)

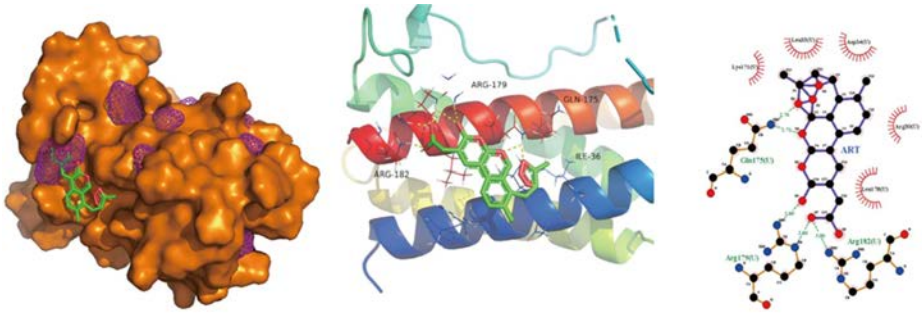

Fig. S2: Docking results of ART monomer molecule and IL6 protein (1ALU)

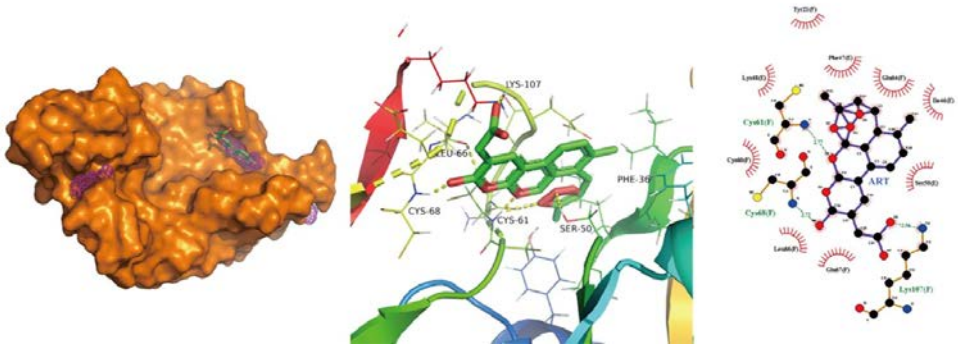

Fig. S3: Docking results of ART monomer molecule and VEGFA protein (5O4E)

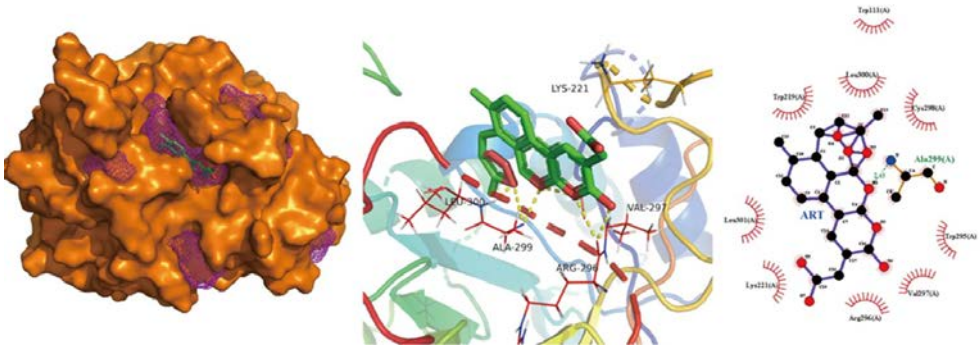

Fig. S4: Docking results of ART monomer molecule and AKR1B1 protein (5OU0)

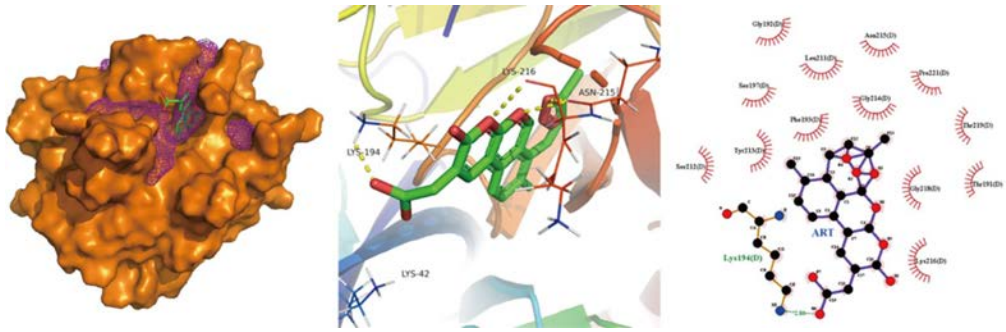

Fig. S5: Docking results of ART monomer molecule and GZMB protein (4GAW)

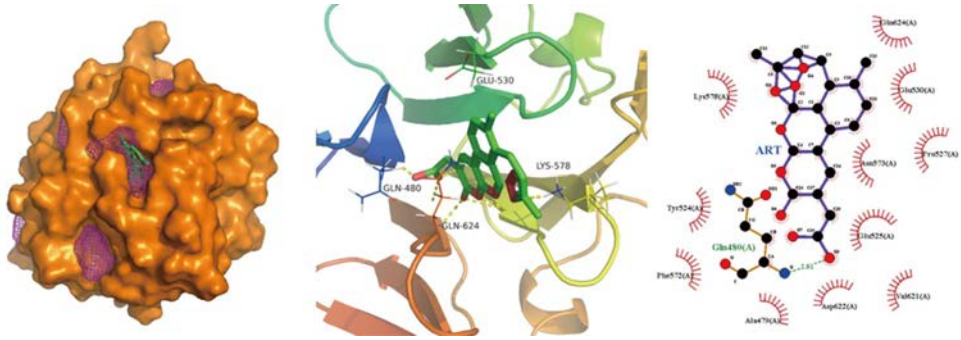

Fig. S6: Docking results of ART monomer molecule and MMP2 protein (1RTG)

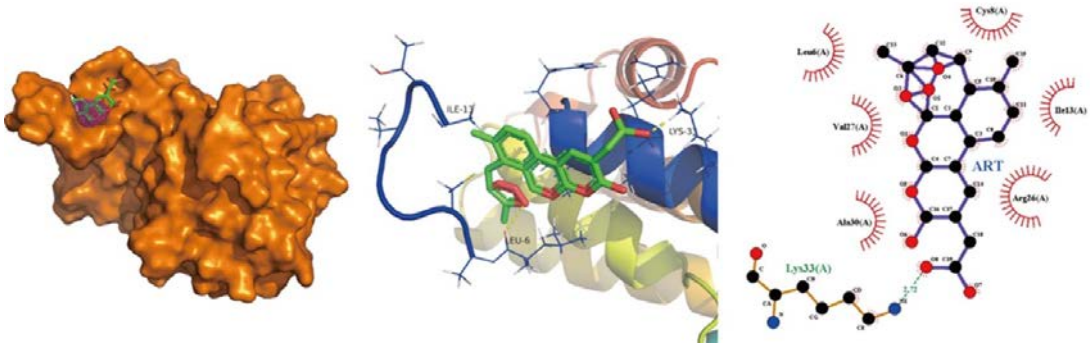

Fig. S7: Docking results of ART monomer molecule and CCND1 protein (2W96)

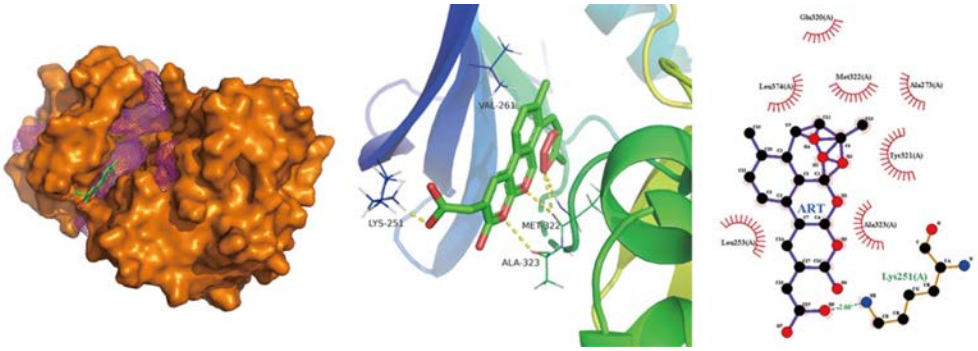

Fig. S8: Docking results of ART monomer molecule and LYN protein (5XY1)

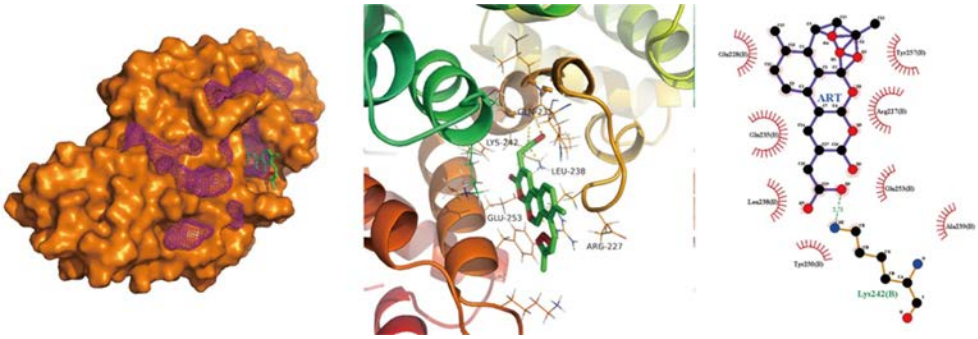

Fig. S9: Docking results of ART monomer molecule and ANXA5 protein (1HAK)

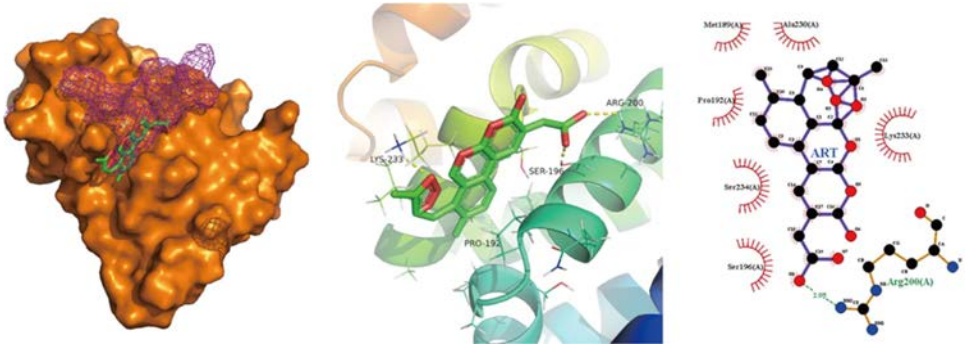

Fig. S10: Docking results of ART monomer molecule and CTNNB1 protein (3SL9)

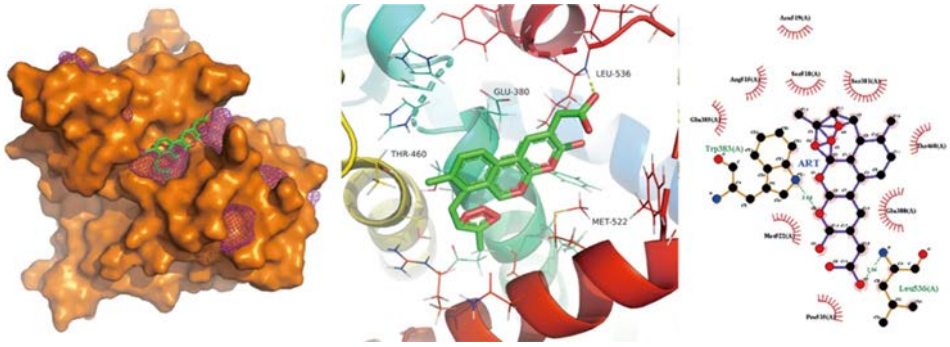

Fig. S11: Docking results of ART monomer molecule and ESR1 protein (2R6W)

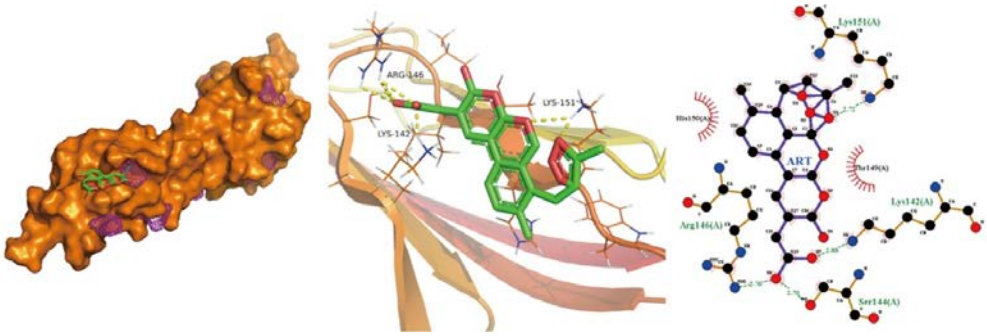

Fig. S12: Docking results of ART monomer molecule and CD2 protein (1HNF)

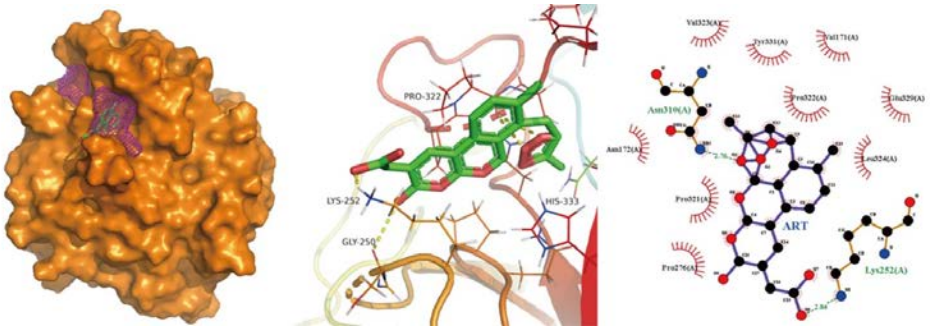

Fig. S13: Docking results of ART monomer molecule and GALM protein (1SNZ)

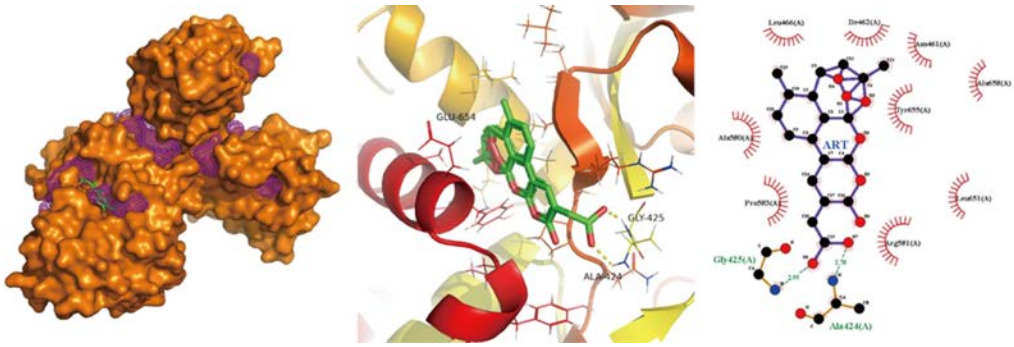

Fig. S14: Docking results of ART monomer molecule and TF protein (5X5P)

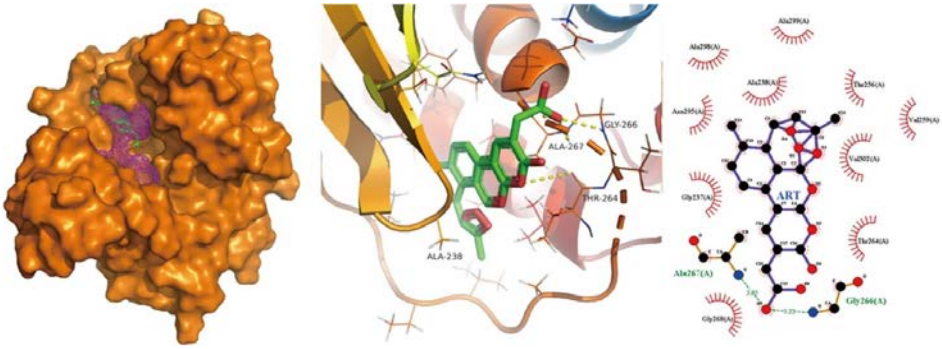

Fig. S15: Docking results of ART monomer molecule and RBKS protein (5BYC)

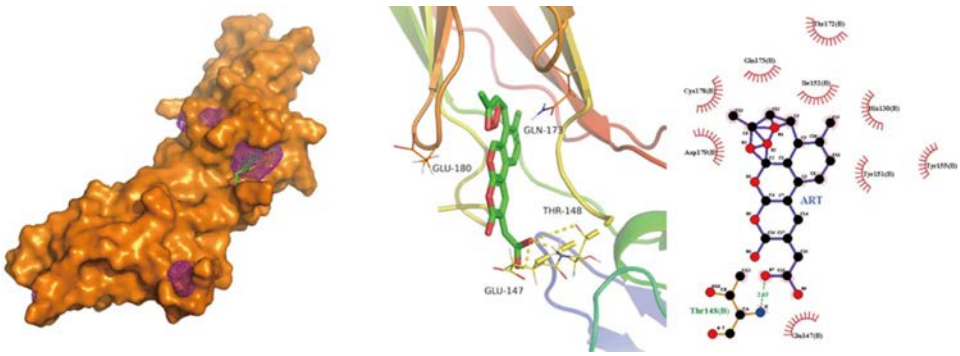

Fig. S16: Docking results of ART monomer molecule and IFNGR1 protein (1FYH)

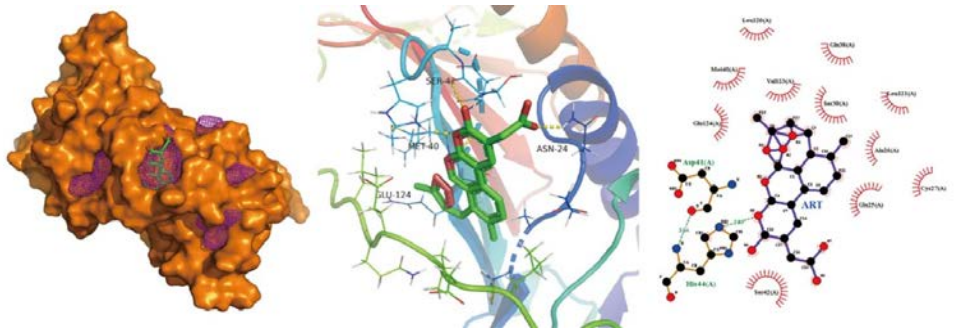

Fig. S17: Docking results of ART monomer molecule and PCNA protein (6HVO)

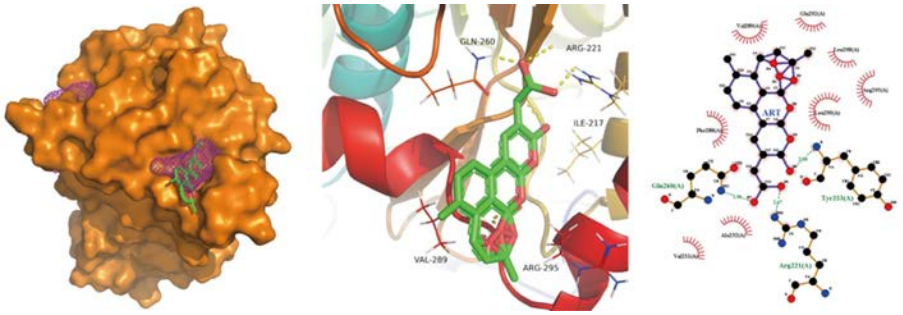

Fig. S18: Docking results of ART monomer molecule and SRM protein (2O05)

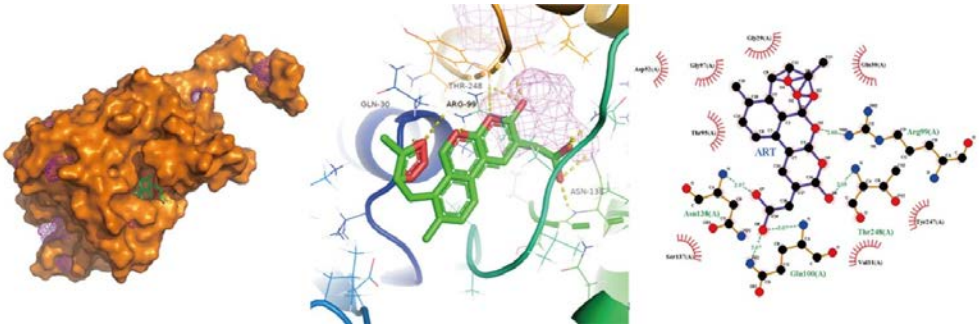

Fig. S19: Docking results of ART monomer molecule and LDHB protein (1T2F)

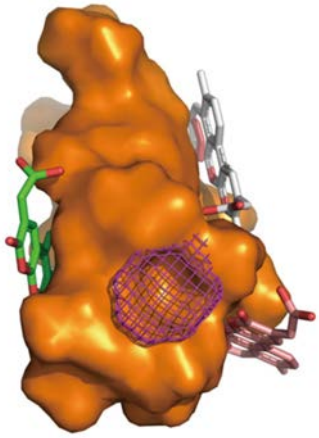

Fig. S20: Docking results of ART monomer molecule and MS4A1 protein (2OSL)